How many dimensions are required to approximate the potential energy landscape of a model protein?

Tamiki Komatsuzaki,[a] Kyoko Hoshino, and Yasuhiro Matsunaga
Nonlinear Science Laboratory, Department of Earth and Planetary Sciences, Faculty of Science, Kobe University, Nada, Kobe 657-8501, Japan

Gareth J. Rylance and Roy L. Johnston[b]
School of Chemistry, University of Birmingham, Edgbaston, Birmingham B15 2TT, United Kingdom

David J. Wales[c]
University Chemical Laboratories, Cambridge CB2 1EW, United Kingdom

(Received 11 October 2004; accepted 7 December 2004; published online 22 February 2005)

A scheme to approximate the multidimensional potential energy landscape in terms of a minimal number of degrees of freedom is proposed using a linear transformation of the original atomic Cartesian coordinates. For one particular off-lattice model protein the inherent frustration can only be reproduced satisfactorily when a relatively large number of coordinates are employed. However, when this frustration is removed in a Gō-type model, the number of coordinates required is significantly lower, especially around the global potential energy minimum. To aid our interpretation of the results we consider modified disconnectivity graphs where a measure of the structural diversity and a metric relation between the stationary points are incorporated. © *2005 American Institute of Physics*. [DOI: 10.1063/1.1854123]

I. INTRODUCTION

The "energy landscape" perspective holds great promise for resolving important contemporary issues in the dynamics and thermodynamics of clusters, liquids, glasses, and biomolecules.[1–5] The observed structures, thermodynamics and dynamics of clusters, and biomolecules are determined by the underlying potential energy surface (PES), which is a function of $3N$ atomic Cartesian coordinates for a system composed of N atoms. However, in providing fundamental explanations for such properties in terms of the underlying PES, there exist two major difficulties. First, the number of stationary points grows exponentially with the number of atoms.[6–8] Second, it may be difficult to project the multidimensional character of the PES onto a low-dimensional space in a manner that faithfully and usefully captures the essential aspects of the problem. For example, Doye[9] has recently reported that the network formed by the minima and saddles on the PES of small clusters has both a small-world and scale-free character.

The most powerful tool currently available for visualizing a high-dimensional PES is probably the disconnectivity graph approach introduced by Becker and Karplus,[10] which has now been applied to a wide range of systems.[4,11] Such graphs are constructed from a database of local minima and index one saddles to which they are connected by steepest-descent paths. Here an index one saddle is defined as a stationary point with precisely one negative Hessian eigenvalue.[12] There are two unique downhill steepest-descent paths that correspond to each index one saddle, and these paths usually lead to local minima (although they can lead to lower energy saddles of index one via branch points).[7] The lowest energy paths between local minima are usually mediated by index one saddles according to the Murrell–Laidler theorem.[13] This theorem applies throughout the present work, since we consider only nonlinear geometries with well-behaved Taylor expansions in Cartesian coordinates.[14] Disconnectivity graphs provide a global view of the PES, which retains topological information. Furthermore, the qualitative appearance of the graph is often sufficient to predict qualitative aspects of the kinetics and thermodynamics, such as multiple relaxation time scales and features in the heat capacity for landscapes containing multiple potential energy funnels.[4]

The focus of the present contribution is the off-lattice three-color, 46-bead BLN model protein of Honeycutt and Thirumalai,[15–18] which has been examined in a number of subsequent studies.[19–32] The original BLN model was designed to exhibit frustration, and it does not fold efficiently.[17–19] Two peaks are seen in the heat capacity, corresponding to collapse from extended to compact states at higher temperature, and to folding into the global potential energy minimum at lower temperature.[17,19] However, when a Gō model[33] is constructed by removing all the attractive interactions that do not correspond to nonlocal closest contacts in the native state, a much sharper single heat capacity peak is observed.[21] In the original model the folding rate also starts to deviate from exponential behavior just below the collapse temperature.[19,21] These observations can all be explained from the corresponding disconnectivity graphs.[23,29] The surface for the original BLN potential includes a number of relatively deep potential energy funnels, reflecting the frustration inherent in the model. However, for the Gō model

[a]Electronic mail: tamiki@kobe-u.ac.jp
[b]Electronic mail: r.l.johnston@bham.ac.uk
[c]Electronic mail: dw34@cam.ac.uk

the surface has an almost ideal single funnel topography,[23] as Nymeyer *et al.* inferred from their studies of folding kinetics.[21]

The databases of stationary points used in the construction of disconnectivity graphs can be used in quantitative calculations of thermodynamic and kinetic properties using the superposition approach, and master equation or kinetic Monte Carlo schemes.[4] One of the aims of the present contribution is to investigate whether further information can usefully be encoded into the disconnectivity graph itself, for example, by employing a physically motivated coordinate for the horizontal axis, instead of simply arranging the graph as clearly as possible. The results can be compared with free energy disconnectivity graphs considered in previous work,[29,34] which include results for the BLN model.[29]

A further aim of this paper is to investigate how many degrees of freedom are needed to provide a useful approximation to the PES, and to employ the corresponding results to visualize the landscape. We present a simple scheme to decompose the $3N$ atomic Cartesian coordinates into combinations that are essential and nonessential in representing the topography of the PES. We find that more degrees of freedom are needed to describe the frustrated landscape of the original BLN model compared to the Gō potential. This intuitive result is expected to have some generality. Disconnectivity graphs are also considered in which the number of local minima in each superbasin and dimensionality of the configuration space belonging to the superbasin are represented, and the horizontal axis corresponds to a collective coordinate that best represents the distribution of stationary points.

II. METHOD

The stationary points of a PES, where the gradient vanishes, provide an insightful way to coarse-grain both kinetics and thermodynamics.[4] In particular, thermodynamic properties can be calculated from a suitable sample of local minima, while global kinetics can be investigated using the minimum-to-minimum rate constants associated with each index one saddle.[4] To capture the topographical features of a multidimensional PES, it is natural to start by scrutinizing the distribution of these stationary points and the connections between them. All the present results were obtained for databases of minima and index one saddles located in previous work.[23] Let the total number of stationary points for a system of N atoms be N_{SP}. To eliminate uncertainties in the definition of the coordinate system, McLachlan's "best fit" prescription[35] is employed to uniquely remove the total translational and rotational degrees of freedom.

(1) Calculate a "reference configuration" defined by an ensemble average $\langle \mathbf{q} \rangle$ of a set of N_{SP} configurations, $\{\mathbf{q}(k)\}$, $\{\mathbf{q}(1), \mathbf{q}(2), \ldots, \mathbf{q}(N_{\mathrm{SP}})\}$, in a given coordinate system whose center of mass is set to be the origin. Here, $q_i(k)$ denotes the ith Cartesian coordinate of the kth stationary point where $i=1,2,\ldots,3N$ and $k=1,2,\ldots,N_{\mathrm{SP}}$.

(2) Make a new set of configurations $\mathbf{q}'$: orient each configuration to put it as close as possible to coincidence with the (fixed) reference configuration $\langle \mathbf{q} \rangle$ by minimizing the sum of residues between $\mathbf{q}'$ and $\langle \mathbf{q} \rangle$, s,

$$s = \frac{1}{2} \sum_{i=1}^{3N} (q_i' - \langle q_i \rangle)^2. \tag{1}$$

(3) Calculate a new ensemble average configuration for $\{\mathbf{q}'(k)\}$.

(4) Define the new ensemble average as the new reference configuration and return to step (2) until the ensemble average configuration is converged within some threshold.

In the present work we have found that McLachlan's best fit procedure requires only five to seven cycles to converge the average structure within $10^{-8}\sigma$. Hereafter we denote $\mathbf{q}(k)$ as the translation-rotation-free configuration space. Let $\mathbf{D}$ be a $3N \times N_{\mathrm{SP}}$ matrix, whose elements D_{ik} are defined as the deviation of the (mass-weighted) ith Cartesian coordinate $q_i(k)$ in the kth sampled configuration from the ensemble average $\langle q_i \rangle$, i.e.,

$$D_{ik} = q_i(k) - \langle q_i \rangle, \tag{2}$$

where

$$\langle q_i \rangle = \frac{1}{N_{\mathrm{SP}}} \sum_{k=1}^{N_{\mathrm{SP}}} q_i(k). \tag{3}$$

Then, using a $3N \times 3N$ variance-covariance matrix $\mathbf{R}$,

$$\mathbf{R} = \frac{1}{N_{\mathrm{SP}}} \mathbf{D}\mathbf{D}^{\mathrm{T}} \tag{4}$$

(where $\mathbf{D}^{\mathrm{T}}$ is the transpose matrix of $\mathbf{D}$), whose second moment element R_{ij} is

$$R_{ij} = \frac{1}{N_{\mathrm{SP}}} \sum_{k=1}^{N_{\mathrm{SP}}} [q_i(k) - \langle q_i \rangle][q_j(k) - \langle q_j \rangle], \tag{5}$$

we can define a set of principal components (PC's) $\mathbf{Q}$ using the eigenvectors $\mathbf{U}$ that diagonalize $\mathbf{R}$:

$$\mathbf{R}\mathbf{U} = \mathbf{U}\mathbf{r} \quad (\mathbf{U}^{\mathrm{T}}\mathbf{U} = \mathbf{I}). \tag{6}$$

The eigenvalue r_i, the ith element of the diagonal matrix $\mathbf{r}$, represents the variance of the ith collective coordinate Q_i,

$$Q_i = \sum_{j=1}^{3N} U_{ji} q_j. \tag{7}$$

The larger the value of r_i, the better Q_i represents the distribution of stationary points in configuration space. The $\mathbf{Q}$ are sorted in order of decreasing variance, $r_1 \geqslant r_2, \ldots, \geqslant r_{3N}$. In the translation-rotation-free system one can always find six zero eigenvalues whose eigenvectors correspond to total translational and rotational motions of the system. Otherwise, the results would depend on the coordinates of the total translational and/or rotational degrees of freedom of the system. This linear transformation is referred to as a principal component analysis (PCA),[36,37] which determines a set of linear, collective coordinates to best represent most fluctuations or distributions of the system. PCA has often been

used to analyze cooperative behavior in protein dynamics.[28,38–40] The complementary approach[41,42] of principal coordinate analysis is obtained by replacing $\mathbf{R}$ in Eq. (4) with an $N_{\mathrm{SP}}\times N_{\mathrm{SP}}$ matrix, $\mathbf{R}=\mathbf{D}^{\mathrm{T}}\mathbf{D}/3N$. This scheme has also been employed by Becker and Karplus,[10] and Elmaci and Berry[26] to visualize the distribution of stationary points in the multidimensional configuration space of proteins.

Here we use the PCA to derive an approximate description of the PES in lower dimensionality. The original Cartesian coordinates are reproduced by

$$\mathbf{q}=\mathbf{U}^{-1}\mathbf{Q}, \tag{8}$$

where $\mathbf{U}\mathbf{U}^{-1}=\mathbf{U}^{-1}\mathbf{U}=\mathbf{I}$, so that

$$q_i=\sum_{j=1}^{3N}U_{ji}^{-1}Q_j=\sum_{j=1}^{3N}U_{ij}Q_j\approx\sum_{j=1}^{N_r}U_{ij}Q_j, \tag{9}$$

where we approximate $\mathbf{q}$ in terms of the first N_r principal components. We can model any PES that can be represented in terms of Cartesian coordinates $\mathbf{q}$ using an approximate form based on the N_r principal components without changing the form of the potential energy function. For instance, if the potential function is described in terms of internal degrees of freedom, e.g., interparticle distances r_{ij}, bond angles θ_{ijk}, and torsional angles Φ_{ijkl}, then the Cartesian coordinates x_i,y_i,z_i of the ith particle define each internal coordinate as

$$r_{ij}=\sqrt{(x_i-x_j)^2+(y_i-y_j)^2+(z_i-z_j)^2}, \tag{10}$$

$$\theta_{ijk}=\cos^{-1}\left(-\frac{\mathbf{r}_{jk}\cdot\mathbf{r}_{ij}}{r_{jk}r_{ij}}\right), \tag{11}$$

and

$$\Phi_{ijkl}=\cos^{-1}\left[\frac{(\mathbf{r}_{jk}\times\mathbf{r}_{ij})\cdot(\mathbf{r}_{kl}\times\mathbf{r}_{jk})}{r_{ij}r_{jk}r_{kl}^2\sin\theta_{ijk}\sin\theta_{jkl}}\right]. \tag{12}$$

III. MODEL PROTEIN

We have employed the three-color, 46-bead BLN model of Honeycutt and Thirumalai[15–18] to illustrate our proposed reduction scheme for multidimensional energy landscapes. This model is composed of hydrophilic (L), hydrophobic (B), and neutral (N) beads, interacting according to the following potential:

$$\begin{aligned}V&=V_{\mathbf{r}}+V_{\boldsymbol{\theta}}+V_{\boldsymbol{\Phi}}+V_{\mathbf{R}}\\&=\sum_{i}^{bonds}K_r(r_i-r_0^i)^2+\sum_{i}^{angles}K_\theta(\theta_i-\theta_0^i)^2\\&\quad+\sum_{i}^{torsional}[A(1+\cos\Phi_i)+B(1+\cos3\Phi_i)]\\&\quad+\sum_{i<j-3}^{nonbonding\ pairs}4\epsilon S_1\left[\left(\frac{\sigma}{R_{ij}}\right)^{12}-S_2\left(\frac{\sigma}{R_{ij}}\right)^{6}\right],\end{aligned} \tag{13}$$

where the van der Waals (vdW) interactions are used to mimic the hydrophilic, hydrophobic, and neutral characters of the beads: $S_1=S_2=1$ for BB (attractive) interactions, $S_1=2/3$ and $S_2=-1$for LL and LB (repulsive) interactions, and $S_1=1$ and $S_2=0$ for all the other pairs involving N, expressing only excluded volume interactions. For the bond-stretching and angle-bending force constants we use $K_r=231.2\epsilon\sigma^{-2}$ and $K_\theta=20\epsilon/\mathrm{rad}^2$, with the equilibrium bond length $r_0^i=\sigma$ and the equilibrium bond angle $\theta_0^i=1.8326$ rad. The units of energy, temperature, the bead mass, time, and frequency are ϵ, ϵ/k_B, M, $t^*=\sigma\sqrt{M/\epsilon}$, and $1/t^*$, unless otherwise noted. The global potential energy minimum for the sequence, $B_9N_3(LB)_4N_3B_9N_3(LB)_5L$, folds into a β-barrel structure with four strands. This structure is ensured by setting up the torsional potential so that there are stiff *trans* preferences in the four strands, while at the loop regions, consisting of neutral beads, the torsional potential has a small barrier with no preference for any of the three rotameric states. In particular, $A=B=1.2\epsilon$, except for torsional angles involving two or more neutral residues where $A=0$ and $B=0.2\epsilon$. The rigid bonds of the original model by Honeycutt and Thirumalai[16] are replaced with stiff but harmonic, springlike bonds.[20]

This BLN model protein has been analyzed in terms of structure,[20,23,26,32] thermodynamics,[19,29] kinetics,[21] and dynamics.[28] The original potential exhibits a rather frustrated PES.[21,23] The effects of frustration may be eliminated by constructing a Gō model where all attractive interactions between pairs of beads that are not in contact in the native state (global minimum) are removed. This transformation is equivalent to setting $S_2=0$ in Eq. (13) for nonbonded pairs of hydrophobic beads separated by more than 1.167σ in the global minimum.[23] This change increases the heterogeneity of the interactions, since it makes the attractive forces more specific. In this paper, we examine both the original BLN model and the less frustrated Gō model. We use 500 minima and 636 saddles for the BLN model, and 520 minima and 844 saddles for the Gō model, which were sampled in a previous study using an eigenvector-following search algorithm.[23] These are relatively small samples compared to more recent studies,[32] but we expect them to be sufficient for the present purposes.

Some recent investigations of the BLN model include construction of free energy disconnectivity graphs and comparison with parallel tempering simulations.[29] Stoycheva *et al.* have also studied the effect of introducing salt bridges (ion pairs) into the BLN potential on folding rates,[31] and Wales and Dewsbury have used disconnectivity graphs to reveal how these bridges affect the underlying PES.[32] Matsunaga and co-workers[28,40] have analyzed time series of potential energy fluctuations and principal components based on instantaneous geometries sampled over a range of temperatures. They found that the stochastic nature of the principal components with large variance tends to be suppressed through a wide range of degrees of freedom at the collapse temperature, although between 70% and 80% of the principal components lose their memory in only a hundred simulation steps.

IV. RESULTS AND DISCUSSIONS

How many PC's are required to reproduce the total variance of the distribution of stationary points in the 138-

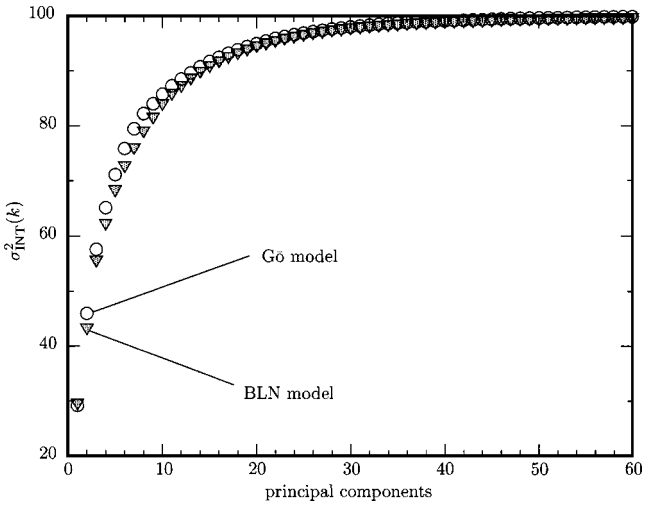

FIG. 1. The ratio of the integrated variance to the total variance $\sigma^2_{\mathrm{INT}}(k)$: the symbols (shaded) $\triangledown$ and $\bigcirc$, respectively, denote the BLN model and the Gō-like BLN model hereafter unless noted otherwise.

dimensional coordinate space? Figure 1 shows the ratio of the integrated variance to the total variance estimated in terms of the first k principal components, $\sigma^2_{\mathrm{INT}}(k)$, defined by

$$\sigma^2_{\mathrm{INT}}(k) = \frac{\sum_i^k r_k}{\sum_i^{3N-6} r_k}, \tag{14}$$

where r_k is the kth eigenvalue of variance-covariance matrix. Roughly 99% of the total variance can be reproduced by the first 40 PC's for both the models, of which the first principal component Q_1 contributes about 30% of the total. As the number of the PC's is increased the behavior of the Gō-like BLN model is reproduced by a smaller number of PC's than the original frustrated model, although the difference becomes negligible above about 40 PC's.

We now consider how the PES's of the BLN and Gō potentials can be approximated by a reduced set of PC's using Eq. (9). Figure 2 shows the difference ΔV between the

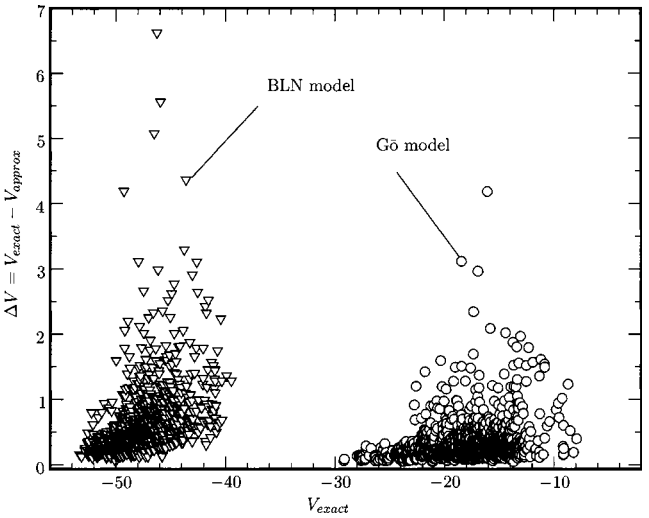

FIG. 2. The energy difference ΔV between the exact V_{exact} and the approximate V_{approx} calculated from the first 92 principal components Q_1–Q_{92}. The energy is in units of ϵ.

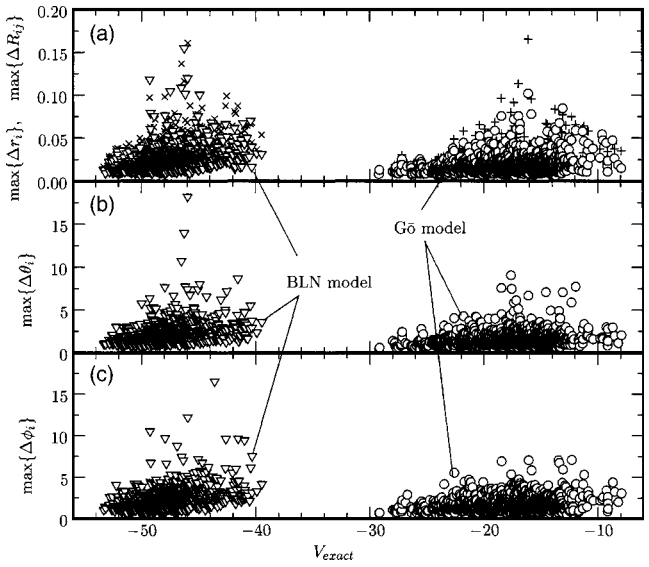

FIG. 3. The maximum deviations between the exact configurations and the approximate configurations obtained from the first 92 principal components. (a) Bonding and nonbonding interparticle separations, $\{\Delta r_i\}$ and $\{\Delta R_{ij}\}$. The symbols $\triangledown$ and $\bigcirc$, and $\times$ and $+$ denote $\{\Delta r_i\}$ and $\{\Delta R_{ij}\}$ of the BLN model and the Gō-like BLN model, respectively. (b) Bending angles $\{\Delta\theta_i\}$. (c) Torsional angles $\{\Delta\Phi_i\}$. The length, angle, and the energy are in units of σ, degrees, and ϵ, respectively.

approximate potential energy V_{approx} evaluated with $N_r=92$ (two thirds of the total number of degrees of freedom) and the exact energies V_{exact} for all the minima and index one saddles of both potentials. Here we note that the density of minima per unit energy is larger for the BLN model than for the Gō model, so that the highest energy minima in the sample are still compact for the BLN model, while for the Gō potential they are significantly unfolded.

The energy range between the lowest and the highest energies is 13.8ϵ (from -53.3ϵ to -39.5ϵ) for the BLN model and 21.3ϵ (from -29.2ϵ to -7.9ϵ) for the Gō model. For both potentials, as the energy of the stationary points increases, the deviation of the approximate potential from the exact value also increases. The minimum and maximum deviations are 0.05ϵ and 6.620ϵ for the original BLN model, and 0.045ϵ and 4.185ϵ for the Gō model. However, the deviations are smaller in the Gō model than for the original potential, especially for stationary points close (in energy) to the global minimum, which are relatively insensitive to the last 46 principal components (from Q_{93} to Q_{138}). Figure 3 shows the maximum deviations in bonding and nonbonding interparticle separations, $\{\Delta r_i\}$ and $\{\Delta R_{ij}\}$, and bending angles $\{\Delta\theta_i\}$ and torsional angles $\{\Delta\Phi_i\}$ between the original configurations and those approximated in terms of the first 92 principal components. Again, as for the energies, the structural deviations are smaller for the Gō model, especially near the global minimum.

The density distribution of stationary points as a function of potential energy V, $P_{\mathrm{SP}}(V)$, and the integral $\int_0^V P_{\mathrm{SP}}(V')dV'$ are plotted for both models in Fig. 4 using an energy bin of width ϵ. Both density distributions can be fitted reasonably well by a Gaussian function, although the fit is better for the original BLN potential and the density distribution of the Gō model deviates from a simple Gaussian distribution in the

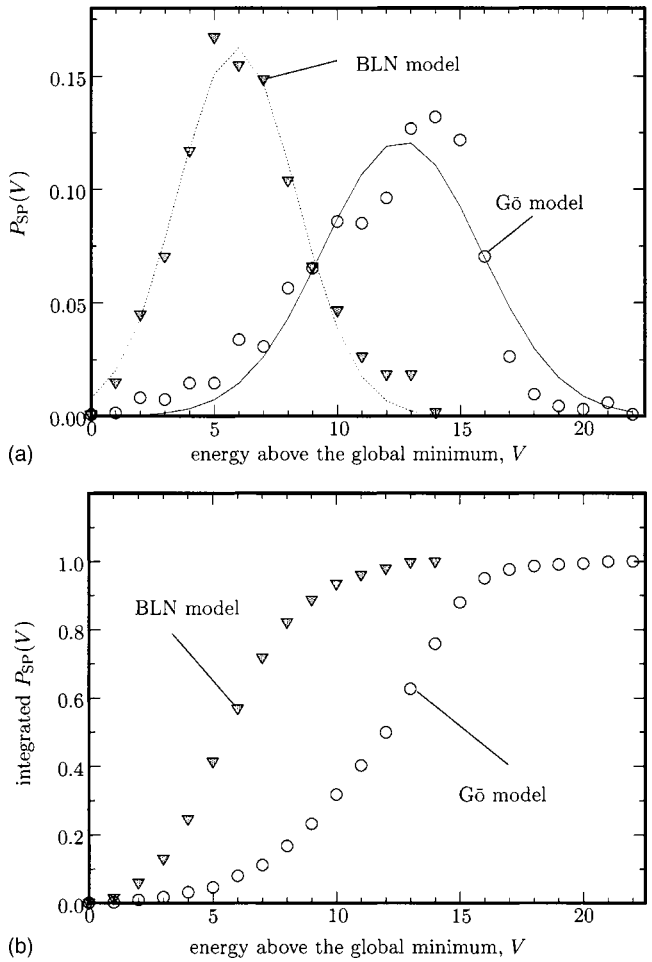

FIG. 4. (a) The density distribution $P_{SP}(V)$ and (b) the integrated density distribution $\int_0^V P_{SP}(V')dV'$ for local minima and index one saddles as a function of energy V relative to that of the global minimum of each model. In (a), the dashed and solid lines denote the best fit Gaussian functions, which are $P_{SP}(V) \simeq 0.16 \exp[-(V-5.9)^2/3.4^2]$ (correlation coefficient 0.989) for the BLN model, and $P_{SP}(V) \simeq 0.12 \exp[-(V-12.6)^2/4.6^2]$ (correlation coefficient 0.951) for the Gō model. The energy is in units of ϵ.

region of the global minimum where the energy landscape was designed to have a strong energy bias. This result implies that the relative contribution of the stationary points employed in calculating the PC's is small in the vicinity of the global minimum. Moreover, the density of stationary points in the vicinity of the global minimum is smaller for the Gō model than the BLN model.

Figures 5 and 6 show the natural logarithm of the product of positive Hessian eigenvalues $\{\lambda_i\}$ for each stationary point as a function of the exact energy V_{exact} and the energy difference ΔV $(=V_{exact}-V_{approx})$, respectively. The product

$$\Lambda = \prod_i^{\lambda>0} \lambda_i \tag{15}$$

is related to the *stiffness* of the stationary point, i.e., how much the energy changes for small displacements of the structure. The units of each λ_i are $\epsilon/m\sigma^2$, and the results considered here correspond to $\epsilon=0.01$, $\sigma=3.4$, and $m=1$. The values of $\ln\Lambda$ for the Gō model are generally smaller than those for the original potential (see Fig. 5). However, as shown in Fig. 6, no clear correlation exists between the stiffness of the stationary points and the energy difference ΔV. For instance, there is a large variation in ΔV around $\ln\Lambda \sim -320$, which corresponds to the global minimum of the Gō model.

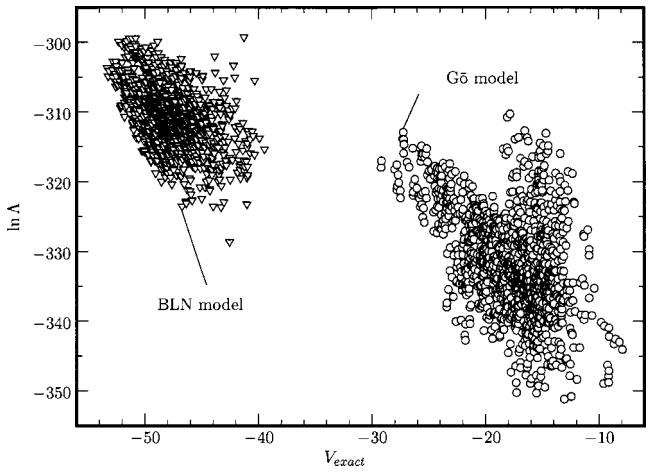

FIG. 5. The natural log of the product of positive Hessian eigenvalues Λ for BLN and Gō models as a function of energy in ϵ.

Structural diversity. Here we introduce two quantities that provide a measure of the structural diversity at energy V. The first function $\sigma_s(V)$ is defined in terms of the variance of the distribution of stationary points:

$$\sigma_s(V) \equiv \frac{1}{N_{SP}(V)} \sum_k^{V_k \leqslant V} \sum_i^{3N} [q_i(k) - \langle q_i \rangle]^2, \tag{16}$$

where $N_{SP}(V)$ denotes the total number of stationary points whose energy is less than V. The second function $D_s(V)$ is defined as the number of principal components (from Q_1 to $Q_{D_s(V)}$) needed to reproduce 99% of the total variance of the distribution of the stationary points whose energies are less than V. Here, we use the translation-rotation-free coordinate system defined in terms of *all* the stationary points, which is consistent with the coordinate system used in approximating the multidimensional potential energy landscape. It was found that even when the translation-rotation-free coordinate system is redefined at each energy V using stationary points

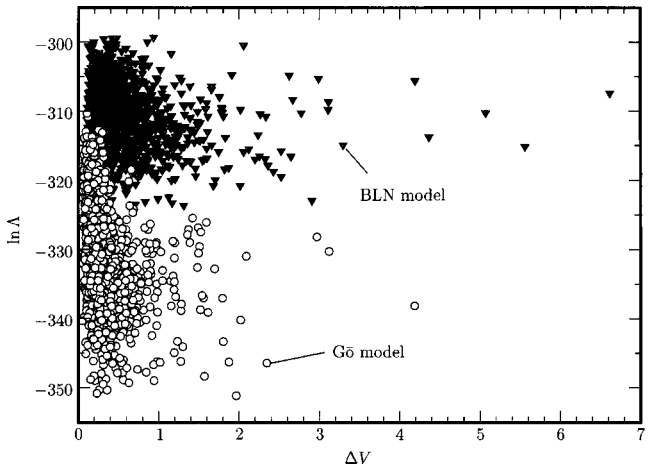

FIG. 6. The natural log of the product of positive Hessian eigenvalues Λ for BLN and Gō models as a function of $\Delta V(=V_{exact}-V_{approx.})$ in ϵ.

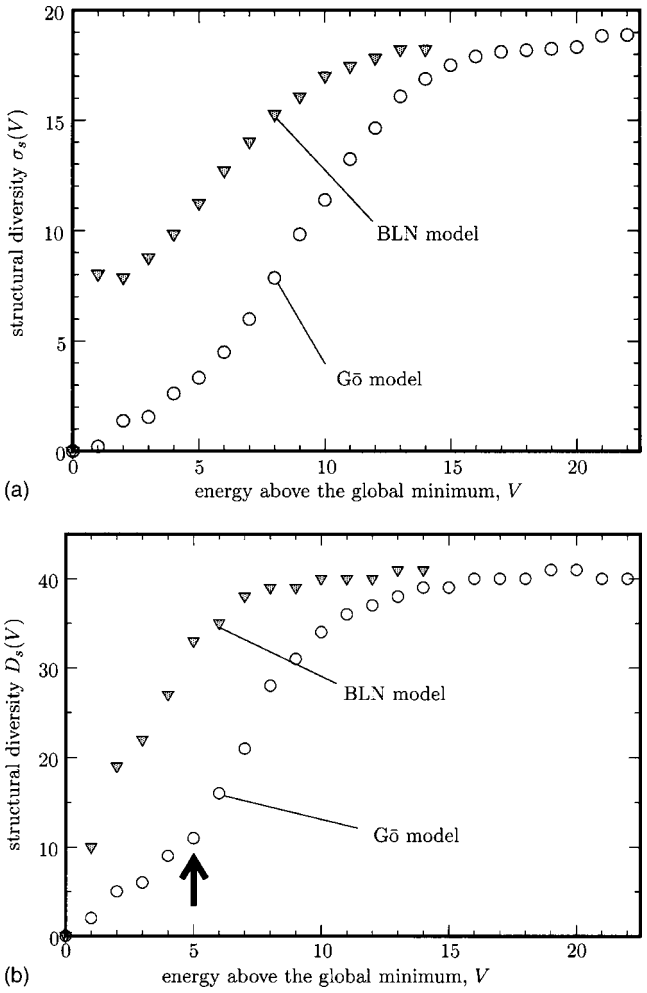

FIG. 7. The structural diversity measures as a function of energy V relative to that of the global minimum of each model: (a) $\sigma_s(V)$ and (b) $D_s(V)$. $\sigma_s(V)$ is in units of σ^2. The arrow in (b) indicates an energy below which both the energies and structures of stationary points are relatively unaffected by one-third of the total number of principal components. See text in detail.

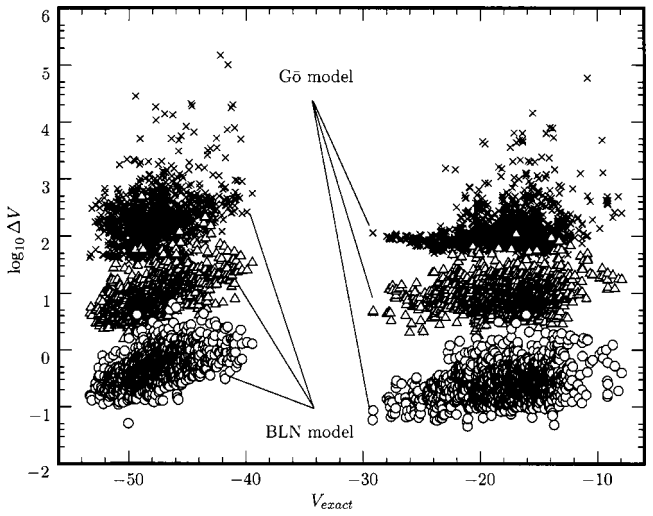

FIG. 8. The energy difference ΔV between the exact V_{exact} and the approximate V_{approx} as a function of V_{exact}: the symbols ◯, ▽ and × denote ΔV calculated from the first 92, 46, and 10 principal components, respectively. The energy is in units of ϵ.

whose energy is smaller than V, both the figures are almost unchanged. Figure 7 shows $\sigma_s(V)$ and $D_s(V)$ as a function of V relative to the global minimum of each model. The two measures of structural diversity are larger for the BLN model than for the Gō model. As V increases to 1ϵ above the global minimum, the first measure $\sigma_s(V)$ increases discontinuously for the BLN model although the second measure $D_s(V)$ increases rather smoothly. In Fig. 7(b), $D_s(V)$ shows a significant change in the dimensionality of configuration space for the Gō model, compared with the BLN model. That is, while $D_s(V)$ increases monotonically from the global minimum energy to a certain converged dimension for the BLN model, $D_s(V)$ for the Gō model does not grow rapidly in the vicinity of the global minimum up to an energy region of $D_s(V) \simeq 10$ [indicated by an arrow in Fig. 7(b)], below which both the energies and structures of stationary points are relatively unaffected by truncation of one third of the total number of degrees of freedom in the principal component space. We believe that this second measure $D_s(V)$, based on the "topographical" dimension of the multidimensional energy landscape, can more properly capture the structural diversity of the system as a function of V, which may also be reflected in the energy density of the local minima. All these results suggest that if the structural diversity grows more rapidly above the native structure, compared to the density of stationary points, then more degrees of freedom are needed to represent the underlying PES.

Energy dependency on the dimensional reduction. So far we have focused on the approximate PES and stationary points in terms of the first 92 principal components. Figure 1 suggests that the energy landscape might be well approximated by around 40 principal components, because these can reproduce 99% of the total variance of the stationary points in the full 138-dimensional configuration space. The approximate energies calculated from the first 10, 46, and 92 principal components are compared in Fig. 8. The energy deviations from the exact energies using the first 10 and 46 principal components lie in the range 33.3ϵ–$148\,675.1\epsilon$, and 1.6ϵ–488.4ϵ for the BLN model, compared to 39.1ϵ–$59\,210.9\epsilon$, and 1.8ϵ–109.0ϵ for the Gō model. In general, the dominant contributions in these energy changes arise from the bond energy terms. The stiff, harmonic spring-like bond energies are responsible for much of the energy difference, even for small deviations in the interparticle separation. For some compact configurations, the nonbonded vdW interaction energy terms make the dominant contribution to the deviation of the approximate energy from the exact value. The energy differences in the bending and the torsional angle energy terms are relatively small compared to these terms.

For the Gō model the approximate potential energies obtained from the first ten principal components are relatively accurate in the vicinity of the global minimum, compared with the other regions (although the ΔV are larger than the energy scale of the stationary points because of the contribution from the bond stretching terms). This result suggests that topographical features of this potential energy funnel can be described reasonably well by only ten degrees of freedom in this region, consistent with Fig. 7(b).

Alternative disconnectivity graphs. Disconnectivity

graphs are usually constructed as follows.[10] At a given discrete series of total energies $V_1 < V_2 < V_3 < \cdots$, the minima can be classified into disjoint sets, termed "superbasins"[11] whose members are mutually accessible, connected by pathways where the energy never exceeds V_i. For every value of V_i each superbasin is represented by a node. Lines are drawn between the nodes at energies V_i and V_{i+1} if they are the same superbasin or they are superbasins that merge at the higher energy V_{i+1}. Here we consider some extensions to this construction, introducing representations of the number of local minima and a topographical dimension for the configuration space in each superbasin, along with physically motivated coordinates for the horizontal axis. In this study the coordinate chosen is the first principal component Q_1. The nodes at energy V_i are placed on the horizontal axis at the average value of the principal coordinate Q_1 for all the points within the superbasin that the node represents. The thickness of the line drawn between merging or identical superbasins is dependent upon the "size" of the superbasin, with a thicker line representing a larger superbasin.

We introduce two kinds of alternative disconnectivity graphs: one indicates the size of superbasin m in terms of the number of stationary points $n_{\mathrm{SP}}(m)$ that belong to it. The other employs the topographical dimension of the superbasin $d_s(m)$ defined by the number of principal components (from Q_1 to $Q_{d_s(m)}$) needed to reproduce 99% of the total variance of the distribution of the stationary points belonging to it. Here we have used the translation-rotation-free coordinate system in calculating the PC's for each superbasin using McLachlan's best fit algorithm. Figure 9 shows the first alternative disconnectivity graph where the thickness of the line reflects the number of stationary points within each superbasin. In the figure, the exact scale of the thickness is defined as follows: first, we normalize the number of stationary points $n_{\mathrm{SP}}(m)$ within each superbasin m by the total number of stationary points N_{SP} to give the thickness parameter w_m. Second, the width of a line $\Delta L(w_m)$ in the graph is determined by

$$\Delta L(w_m) = \begin{cases} \alpha w_m & \text{if } w_m \leqslant 0.15, \\ \log(\alpha w_m) + \beta & \text{if } w_m > 0.15, \end{cases} \tag{17}$$

with $1/N_{\mathrm{SP}} \leqslant w_m \leqslant 1$, $\alpha = 10 \times [\max\{Q_1(k)\} - \min\{Q_1(k)\}]$ and $\beta = 13.83$ (the β value was defined so as to connect the above two equations at $w_m = 0.15$).

Figure 10 shows the second version of the alternative disconnectivity graph, where the thickness of the line reflects the structural diversity $d_s(m)$ within each superbasin. In the figure, we define $w_m = [d_s(m)+1]/D_{max}$, where D_{max} is $3N-6$. The width of the line in the graph is then

$$\Delta L(w_m) = \alpha w_m, \tag{18}$$

with $1/D_{max} \leqslant w_m \leqslant 1$ and $\alpha = 5 \times [\max\{Q_1(k)\} - \min\{Q_1(k)\}]$.

Figures 9 and 10 both clearly show the difference between the single funnellike topography of the Gō-like model and the frustrated topography of the BLN model, which contains many deep superbasins. Thus, the Gō model exhibits a single thick branch in the disconnectivity graphs, Figs. 9(b) and 10(b), corresponding to a single funnel landscape. For the frustrated BLN model, Figs. 9(a) and 10(a), the multiple superbasin nature is manifested in the multiple thick branches. The entanglement implies that similar regions of configuration space are disconnected from each other by high barriers.

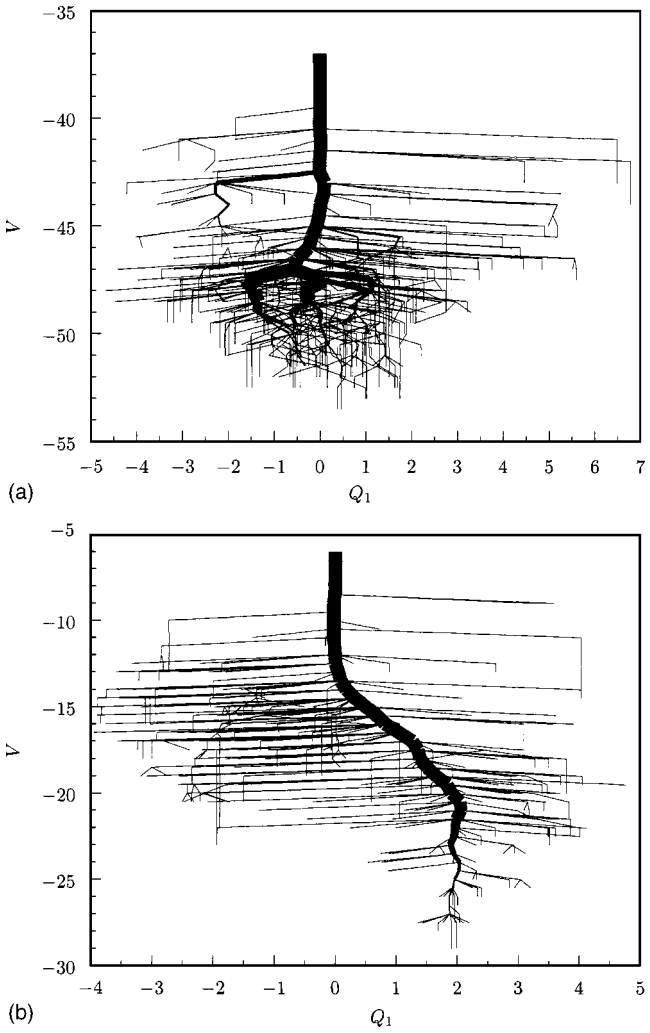

FIG. 9. Alternative disconnectivity graphs. (a) BLN model and (b) Gō model. The thickness of the lines is defined by the number of stationary points $n_{\mathrm{SP}}(m)$ within superbasin m. See text in detail. The horizontal axis is the first principal component. The energy and length are in units of ϵ and σ, respectively.

The spread of points along the first principal component Q_1 near the global minimum is much reduced in the Gō model. In particular, the distribution of the stationary points narrows in terms of Q_1 below an energy of about -23ϵ for the Gō model. This corresponds exactly to a region where both the energies (Fig. 2) and structures (Fig. 3) of the stationary points are unaffected by the last one-third of the total number of principal components, and also where the structural diversity of the superbasins reduces rapidly as V decreases (see Fig. 7).

V. CONCLUSIONS

In this contribution we have investigated reduced dimensionality representations of the multidimensional potential energy landscape and presented a new quantity to measure

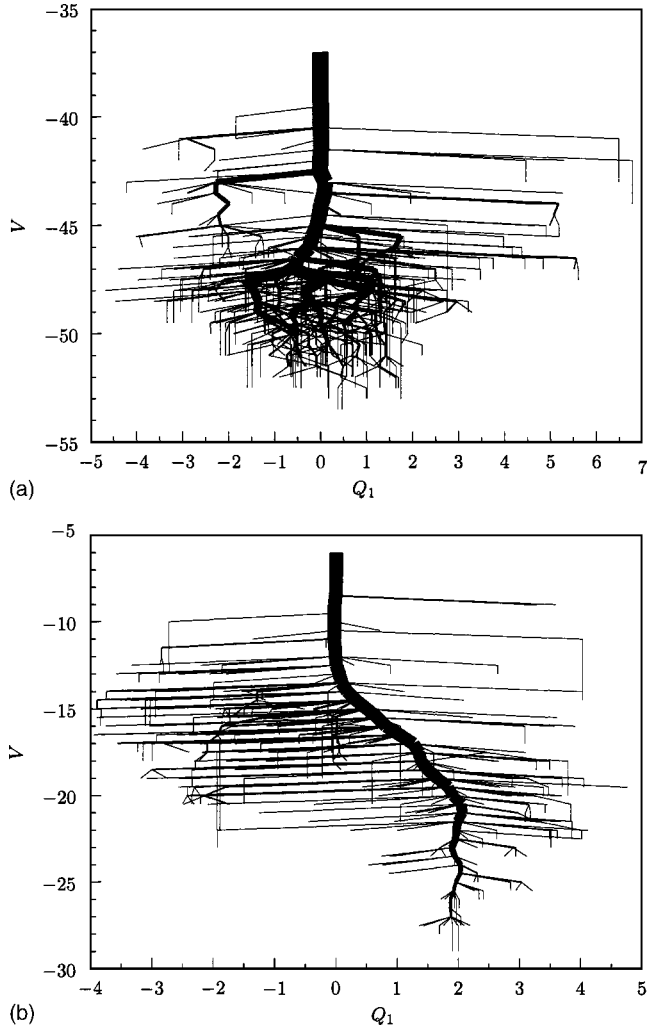

FIG. 10. Alternative disconnectivity graphs. (a) BLN model and (b) Gō model. The thickness of the lines is defined by the structural diversity $d_s(m)$ within superbasin m. See text for details. The horizontal axis is the first principal component. The energy and length are in units of ϵ and σ, respectively.

the structural diversity as a function of energy on the configuration space. We have also considered disconnectivity graphs that incorporate the structural diversity of the stationary points along with a metric relationship between them. We found that the relatively unfrustrated "funnel" energy landscape for the Gō model is less affected by the removal of the last one third of the principal components, compared with the original potential, especially in the vicinity of the global minimum. Our alternative disconnectivity graphs provide useful measures of the number of local minima and their structural diversity. The results suggest that landscapes consisting of a single potential energy funnel are more faithfully reproduced in a lower dimensional space around the global minimum, than are frustrated systems. The latter property may also make the global minimum more robust to perturbations in the potential.

Although in the present paper we have mainly focused on the distinctive characteristics between the simplified funnel landscape and the unbiased more complex landscape, our reduced dimensionality analysis should provide us with a new means to determine to what extent the complexity and dimensional reducibility of energy landscapes depend on the nature and topology of interactions and the size of the system, for a variety of problems, including Lennard–Jones and Morse clusters, polymers, and proteins. Our modified disconnectivity graph can easily compare the size of each superbasin using the metric relationship, even for a set of superbasins from different systems. It is also straightforward to extend these two-dimensional disconnectivity graphs to three-dimensional ones with the x and y axes as the first *two* principal components, where the size of the superbasins are represented as cylinders or tubes.

Our results are based on PCA. PCA is one of the most versatile tools available to address the question of which coordinates or projections best reproduce the properties of the underlying multidimensional PES.[28] As pointed out in previous work,[40] the extent to which the PCA actually represents the PES, and its dynamics, depends on the similarity of the distribution of the original data set to a Gaussian form.

Figure 1 tells us that the first PC can only recover about 30% of the total variance of the distribution of stationary points for both the models considered (the first two PC's recover about 43% and 46% for the BLN and the Gō models, respectively). This result implies that, even though a low-dimensional PCA may semiquantitatively capture topographical features of the underlying PES, it cannot properly represent the true complexity of the *multidimensional* energy landscape, where the system may move from one (super) basin to another through curved or meandering paths. The question of whether a given multidimensional data set can be usefully represented in a lower dimensional space is also a central issue in data mining and pattern recognition studies.[43] It also has important implications for the construction of free energy surfaces using global order parameters, and whether one can usefully project multidimensional potential energy landscapes onto such a subspace.

The principal curve and surface[43] (and also nonmetric multidimensional scaling[44]) are probably the most promising techniques to go beyond the restriction of linear algebra in reducing the multidimensionality of a data set corresponding to a "nonGaussian" distribution. Although such techniques would improve the fraction of the true variance recovered in a lower-dimensional representation, they generally involve nonlinear optimization to extract *nonlinear* components *mode by mode* up to a desired dimension. Hence, although such techniques might improve the "one-dimensional" horizontal axis of a disconnectivity graph, PCA is probably still the most versatile means to address the question of *multidimensionality* in the underlying energy landscape of proteins, because the linear transformation has a unique solution.

ACKNOWLEDGMENTS

The authors would like to thank Dr. Mark A. Miller for providing them with his database of stationary points for the 46 bead model protein and for his valuable comments. T.K. acknowledges support from the Japan Society for the Promotion of Science (JSPS), Grant-in-Aid for Research on Priority Areas "Genome Information Science" and "Control of Molecules in Intense Laser Fields" of the Ministry of Education,

Science, Sports and Culture of Japan, Sumitomo Foundation of Science, and 21st century COE (Center of Excellence) of "Origin and Evolution of Planetary Systems (Kobe University)," MEXT. Y.M. expresses his gratitude to JSPS for JSPS research Fellowships for Young Scientists. R.L.J. and G.J.R. acknowledge support from the Royal Society (Japan-UK Joint Project No. 15208) and the EPSRC.

[1]J. N. Onuchic, P. G. Wolynes, Z. Luthey-Schulten, and N. D. Socci, Proc. Natl. Acad. Sci. U.S.A. **92**, 3626 (1995).
[2]J. D. Bryngelson, J. N. Onuchic, N. D. Socci, and P. G. Wolynes, Proteins: Struct., Funct., Genet. **21**, 167 (1995).
[3]C. M. Dobson, A. Šali, and M. Karplus, Angew. Chem., Int. Ed. **37**, 868 (1998).
[4]D. J. Wales, *Energy Landscapes: With Applications to Clusters, Biomolecules and Glasses* (Cambridge University Press, Cambridge, 2003).
[5]D. J. Wales, J. P. K. Doye, M. A. Miller, P. N. Mortenson, and T. R. Walsh, Adv. Chem. Phys. **115**, 1 (2000).
[6]F. H. Stillinger and T. A. Weber, Science **225**, 983 (1984).
[7]J. P. K. Doye and D. J. Wales, J. Chem. Phys. **116**, 3777 (2002).
[8]D. J. Wales and J. P. K. Doye, J. Chem. Phys. **119**, 12409 (2003).
[9]J. P. K. Doye, Phys. Rev. Lett. **88**, 238701 (2002).
[10]O. M. Becker and M. Karplus, J. Chem. Phys. **106**, 1495 (1997).
[11]D. J. Wales, M. A. Miller, and T. R. Walsh, Nature (London) **394**, 758 (1998).
[12]P. G. Mezey, *Potential Energy Hypersurfaces* (Elsevier, Amsterdam, 1987), p. 69.
[13]J. N. Murrell and K. J. Laidler, Trans. Faraday Soc. **64**, 371 (1968).
[14]D. J. Wales and R. S. Berry, J. Chem. Soc., Faraday Trans. **88**, 543 (1992).
[15]J. D. Honeycutt and D. Thirumalai, Proc. Natl. Acad. Sci. U.S.A. U.S.A. **87**, 3526 (1990).
[16]J. D. Honeycutt and D. Thirumalai, Biopolymers **32**, 695 (1992).
[17]Z. Y. Guo and D. Thirumalai, Biopolymers **36**, 83 (1995).
[18]Z. Y. Guo and D. Thirumalai, J. Mol. Biol. **263**, 323 (1996).
[19]Z. Guo, C. L. Brooks, and E. M. Boczko, Proc. Natl. Acad. Sci. U.S.A. **94**, 10161 (1997).
[20]R. S. Berry, N. Elmaci, J. P. Rose, and B. Vekhter, Proc. Natl. Acad. Sci. U.S.A. U.S.A. **94**, 9520 (1997).
[21]H. Nymeyer, A. E. García, and J. N. Onuchic, Proc. Natl. Acad. Sci. U.S.A. U.S.A. **95**, 5921 (1998).
[22]J. E. Shea, Y. D. Nochomovitz, Z. Y. Guo, and C. L. Brooks, J. Chem. Phys. **109**, 2895 (1998).
[23]M. A. Miller and D. J. Wales, J. Chem. Phys. **111**, 6610 (1999).
[24]B. Vekhter and R. S. Berry, J. Chem. Phys. **110**, 2195 (1999).
[25]B. Vekhter and R. S. Berry, J. Chem. Phys. **111**, 3753 (1999).
[26]N. Elmaci and R. S. Berry, J. Chem. Phys. **110**, 10606 (1999).
[27]J.-E. Shea, J. N. Onuchic, and C. L. Brooks, J. Chem. Phys. **113**, 7663 (2000).
[28]Y. Matsunaga, K. S. Kostov, and T. Komatsuzaki, J. Phys. Chem. A **106**, 10898 (2002).
[29]D. A. Evans and D. J. Wales, J. Chem. Phys. **118**, 3891 (2003).
[30]S. Brown, N. J. Fawzi, and T. Head-Gordon, Proc. Natl. Acad. Sci. U.S.A. **100**, 10712 (2003).
[31]A. D. Stoycheva, J. N. Onuchic, and C. L. Brooks, J. Chem. Phys. **119**, 5722 (2003).
[32]D. J. Wales and P. E. J. Dewsbury, J. Chem. Phys. **121**, 10284 (2004).
[33]Y. Ueda, H. Taketomi, and N. Gō, Biopolymers **17**, 1531 (1978).
[34]S. V. Krivov and M. Karplus, J. Chem. Phys. **117**, 10894 (2002).
[35]A. D. McLachlan, J. Mol. Biol. **128**, 49 (1979).
[36]*Computational Biochemistry and Biophysics*, edited by O. M. Becker, J. A. D. MacKerell, B. Roux, and M. Watanabe (Marcel Dekker, New York, 2001).
[37]R. M. Levy, A. R. Srinivasan, W. K. Olson, and J. A. McCammon, Biopolymers **23**, 1099 (1984).
[38]A. Kitao, F. Hirata, and N. Gō, Chem. Phys. **158**, 447 (1991).
[39]A. Kitao and N. Gō, Curr. Opin. Struct. Biol. **9**, 164 (1999).
[40]T. Komatsuzaki, K. Hoshino, and Y. Matsunaga, Adv. Chem. Phys. **130B**, 257 (2005).
[41]J. C. Gower, Biometrika **53**, 325 (1966).
[42]J. C. Gower, Biometrika **55**, 582 (1968).
[43]T. Hastie, R. Tibshirani, and J. Friedman, *The Elements of Statistical Learning: Data Mining, Inference, and Prediction* (Springer, New York, 2001).
[44]Y. H. Taguchi and Y. Oono, Adv. Chem. Phys. **130B**, 315 (2005).